Title

A mutation in IFT43 causes non-syndromic recessive retinal degeneration

Journal

Human Molecular Genetics, 26(23)

ISSN

0964-6906

Authors

Biswas, Pooja

Duncan, Jacque L

Ali, Muhammad

et al.

Publication Date

2017-12-01

DOI

10.1093/hmg/ddx356

Peer reviewed

Human Molecular Genetics, 2017, Vol. 26, No. 23 4741–4751

doi: 10.1093/hmg/ddx356
Advance Access Publication Date: 18 September 2017
Original Article

ORIGINAL ARTICLE

A mutation in *IFT43* causes non-syndromic recessive retinal degeneration

Pooja Biswas[1,2], Jacque L. Duncan[3], Muhammad Ali[4], Hiroko Matsui[5], Muhammad Asif Naeem[6], Pongali B. Raghavendra[2,7], Kelly A. Frazer[5,8], Heleen H. Arts[9], Sheikh Riazuddin[6,10,11], Javed Akram[10,11], J. Fielding Hejtmancik[12], S. Amer Riazuddin[4,*] and Radha Ayyagari[1,*]

[1]Shiley Eye Institute, University of California San Diego, La Jolla, CA, USA, [2]School of Biotechnology, REVA University, Bengaluru, Karnataka, India, [3]Department of Ophthalmology, University of California San Francisco, San Francisco, CA, USA, [4]The Wilmer Eye Institute, Johns Hopkins University School of Medicine, Baltimore, MD, USA, [5]Institute for Genomic Medicine, University of California San Diego, La Jolla, CA, USA, [6]National Centre of Excellence in Molecular Biology, University of the Punjab, Lahore, Pakistan, [7]School of Regenerative Medicine, Manipal University, Bangalore, India, [8]Department of Pediatrics, Division of Genome Information Sciences, Rady Children's Hospital, San Diego, CA, USA, [9]Department of Pathology and Molecular Medicine, McMaster University, Hamilton, ON, Canada, [10]Allama Iqbal Medical College, University of Health Sciences Lahore, Pakistan, [11]National Centre for Genetic Diseases, Shaheed Zulfiqar Ali Bhutto Medical University, Islamabad, Pakistan and [12]Ophthalmic Genetics and Visual Function Branch, National Eye Institute, NIH, Bethesda, MD, USA

*To whom correspondence should be addressed at: The Wilmer Eye Institute, John Hopkins University School of Medicine, Baltimore, MD 21287, USA. Tel: 410 9553656; Fax: 4109553656; Email: riazuddin@jhmi.edu (S.A.R.); Shiley Eye Institute, University of California San Diego, 9415 Campus Point Drive, JRC 206, La Jolla, CA 92093, USA. Tel: 858 5349029; Fax: 858 2460568; Email: rayyagari@ucsd.edu (R.A.)

Abstract

The aim of this work is to identify the molecular cause of autosomal recessive early onset retinal degeneration in a consanguineous pedigree. Seventeen members of a four-generation Pakistani family were recruited and underwent a detailed ophthalmic examination. Exomes of four affected and two unaffected individuals were sequenced. Variants were filtered using exomeSuite to identify rare potentially pathogenic variants in genes expressed in the retina and/or brain and consistent with the pattern of inheritance. Effect of the variant observed in the gene Intraflagellar Transport Protein 43 (*IFT43*) was studied by heterologous expression in mIMCD3 and MDCK cells. Expression and sub-cellular localization of *IFT43* in the retina and transiently transfected cells was examined by RT-PCR, western blot analysis, and immunohistochemistry. Affected members were diagnosed with early onset non-syndromic progressive retinal degeneration and the presence of bone spicules distributed throughout the retina at younger ages while the older affected members showed severe central choroidal atrophy. Whole-exome sequencing analysis identified a novel homozygous c.100 G > A change in *IFT43* segregating with retinal degeneration and not present in ethnicity-matched controls. Immunostaining showed IFT43 localized in the photoreceptors, and to the tip of the cilia in transfected mIMCD3 and MDCK cells. The cilia in mIMCD3 and MDCK cells expressing mutant *IFT43* were found to be significantly shorter ($P < 0.001$) than cells expressing wild-type *IFT43*. Our studies identified a novel

Received: March 27, 2017. **Revised:** September 8, 2017. **Accepted:** September 12, 2017

homozygous mutation in the ciliary protein *IFT43* as the underlying cause of recessive inherited retinal degeneration. This is the first report demonstrating the involvement of *IFT43* in retinal degeneration.

Introduction

Retinal degeneration is a group of inherited conditions that cause irreversible vision loss (1,2). These segregate in autosomal dominant, recessive, X-linked, and mitochondrial patterns (3–6). Retinal degeneration has also been observed to be a component of a large number of inherited syndromic diseases. More than 250 genes have been implicated in retinal degeneration. The majority of these are associated with non-syndromic inherited retinal degeneration (IRD), and some are associated with both syndromic and non-syndromic forms of retinal degeneration (4,7,8). An example of a gene that is implicated in both isolated and syndromic retinal degeneration is *BBS5* (9,10). The syndrome that is caused by mutations in this gene is known as Bardet-Biedl syndrome, which is part of the ciliopathy spectrum of disorders. Ciliopathies are a group of genetically and phenotypically heterogeneous conditions caused by dysfunction of primary cilia present in a majority of vertebrate cell types (11–13). The phenotype of these diseases spans a wide spectrum of clinical entities involving nearly all organ systems. Bardet-Biedl syndrome, Joubert syndrome and Sensenbrenner syndrome are all examples of ciliary disorders in which retinal dystrophy may occur. That said, while retinal degeneration is a common feature in Bardet-Biedl and Joubert syndrome, it is much less common in Sensenbrenner syndrome as only a few individuals with retinal degeneration have been reported to date (11,14–18).

Sensenbrenner syndrome, also known as cranio ectodermal dysplasia (CED) and short rib polydactyly syndrome (SRPS) belong to a group of autosomal recessive skeletal dysplasias. These disorders are primarily characterized by skeletal and ectodermal abnormalities, chronic renal failure, heart defects and hepatic fibrosis (19,20). The skeletal dysplasias are genetically heterogeneous and in some cases caused by disruption of intraflagellar transport (IFT) (19,20). One of the genes associated with CED and SRPS phenotypes is *IFT43*. A homozygous initiation codon mutation (c.1 A > G) in *IFT43* was previously reported in two affected members of a consanguineous family of Moroccan descent with CED (21). The same mutation has also been observed to segregate with SRPS in the homozygous state in an additional family (20). This mutation is known to disrupt IFT-A complex regulated retrograde transport (11,21). In addition, a homozygous missense mutation, p.Trp179Arg has been reported in a European pedigree with SRPS (20). The cases with SRPS phenotype and *IFT43* mutations were evaluated at 18 weeks gestational age and hence the impact of these mutations on the retina is not known. However, it is remarkable that retinal degeneration was not found in either of the affected children in the Moroccan family as we report here, where non-syndromic early-onset recessive retinal degeneration in a large consanguineous Pakistani pedigree is associated with homozygosity for the c.100 G > A (p.Glu34Lys) *IFT43* mutation. These findings along with functional validation demonstrate the involvement of *IFT43* in non-syndromic recessive early onset retinal degeneration.

Results

Clinical evaluation of patients

Clinical analysis on four affected members (III: 1, III: 2, III: 7 and III: 8) and two unaffected members (III: 4 and III: 5) of this pedigree (Fig. 1) showed normal physical development, body mass index and had no symptoms of Sensenbrenner syndrome such as polydactyly, short-rid or micromelia. All four affected members were reported to have noticeable night vision abnormalities under the age of 5 years. Fundoscopy of affected individuals (III: 1 and III: 8) (Fig. 2) showed optic nerve pallor, retinal vessel attenuation, and bone spicule pigmentary change anterior to the arcades and in the nasal retina at the age of 30 and 23 years, respectively (Fig. 2). III: 1 also had extensive RPE and choroidal atrophy in each macula; III: 8 had a smaller area of RPE and choroidal atrophy in the macula whereas fundoscopy of a control individual was normal at the age of 32 years (Fig. 2). Full field ERG responses were undetectable to all stimulus conditions in all affected individuals when measured at age 46 (III: 1), 42 (III: 2), 46 (III: 7) and 28 (III: 8) years of age, while an unaffected individual exhibited rod and cone responses within normal ranges at age 30 (III: 4) (Fig. 3).

Exome sequencing and analysis of variants

Exomes of four affected (II: 11, II: 12, III: 2 and III: 7) and two unaffected (II: 10 and II: 13) members of the PKRD272 pedigree were captured and sequenced using Nimblegen V2 or V3 sequencing kits. The average base read depth was 99 and the coverage of target sequence ranged from 94 to 99% at 20X. Sequence analysis identified on average 61, 000 variants in each exome. Homozygosity mapping revealed a 18 Mb region on chromosome 14 (chr14: 59000001-77000000) shared by four affected individuals in the homozygous state (Fig. 4A). This region contains 138 genes including *RDH11*, *RDH12* and *TTLL5* genes associated with IRD. However, no rare potentially pathogenic variants segregating with IRD in PKRD272 were observed in these three genes. Further analysis of single nucleotide variants (SNVs) and insertion-deletion (INDELs) variants from six members of this family using in-house exomeSuite software (22) identified 180 homozygous variants that were shared by the four affected individuals and heterozygous or absent in the two unaffected members. Further filtering of these for rare (<0.005 frequency) and potentially pathogenic variants in genes expressed in the retina or brain tissue identified two rare candidate variants for the retinal degeneration in this pedigree (23). One candidate variant was c.100 G > A (p.Glu34Lys) in *IFT43* and the second candidate variant was c.1256 G > C (p.Ser419Thr) in the *SLC38A6* gene. Both changes were located on chromosome 14 about 15 Mb base pairs apart and within the 18 Mb shared homozygous region identified by homozygosity mapping. Both variants are rare, with a frequency of 0.0001 for the *IFT43* variant (rs140366557) and 0.000008 for the *SLC38A6* variant (rs762713377). Among these, only the c.100 G > A (p.Glu34Lys) change in *IFT43* segregated with the retinal degeneration phenotype after analysis of additional members of the PKRD272 pedigree (Fig. 1 and 4B). The glutamic acid residue of p.Glu34Lys is located in a domain that is highly conserved in mammals (Fig. 5A). However, the Chlamydomonas and Drosophila orthologs of *IFT43* showed 39% and 22% homology respectively with the human *IFT43* (Fig. 5A). The p.Glu34Lys change in *IFT43* is predicted to be damaging by PolyPhen2, SIFT and MutationTaster (24,25). These data indicate that this potentially pathogenic variant is the likely cause of retinal dystrophy in the Pakistani family PKRD272. Analysis of 150 ethnicity-matched controls by Sanger sequencing and screening

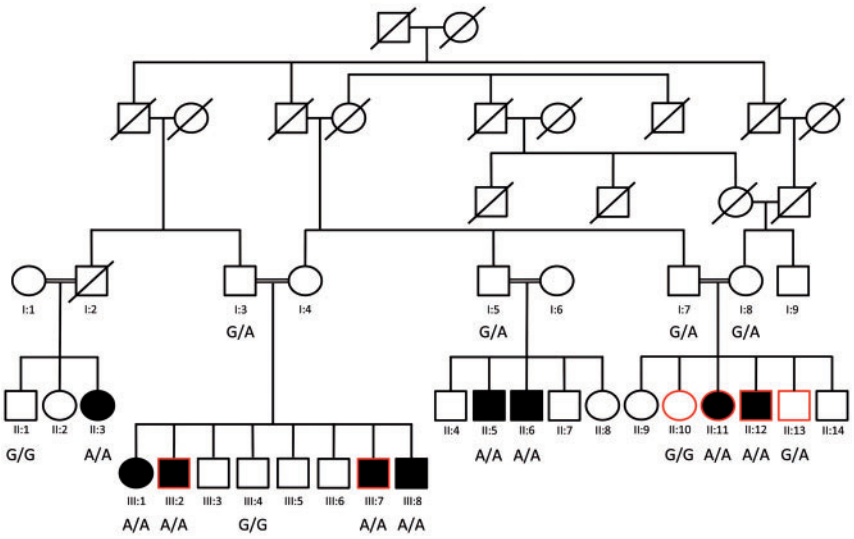

Figure 1. Segregation analysis of *IFT43* c.100 G > A (p.Glu34Lys) variant in PKRD272 pedigree. Segregation of *IFT43* c.100 G > A mutation in pedigree PKRD272 is shown by presenting the genotypes at this locus. Individuals selected for exome sequencing are shown with red outline.

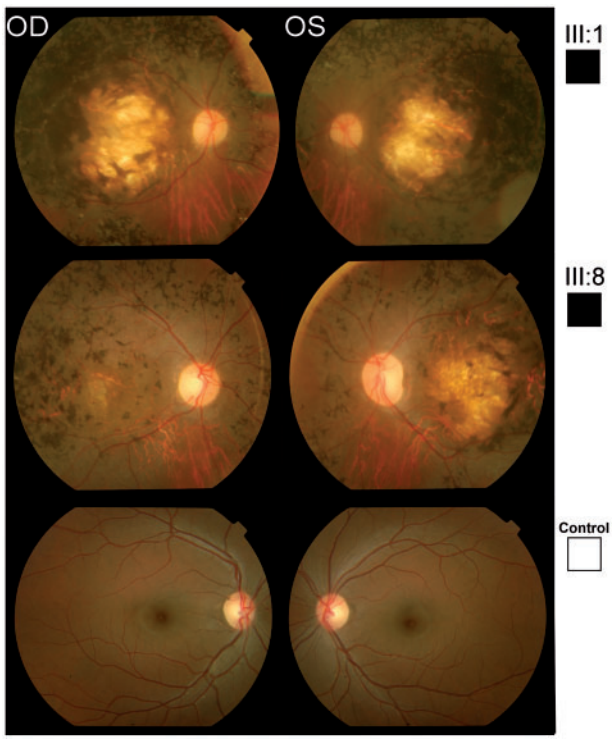

Figure 2. Fundus images from pedigree PKRD272. Fundus images of two affected and one unaffected member. Fundus images of affected individuals (III: 1 and III: 8) showed optic nerve pallor, retinal vessel attenuation, and bone spicule pigmentary change anterior to the arcades and in the nasal retina at the age of 23 and 30 years, respectively. III: 1 had extensive RPE and choroidal atrophy in each macula; III: 8 had a smaller area of RPE and choroidal atrophy in the macula. Color fundus photos of the normal control are without disc pallor, vascular attenuation, pigmentary change or macular RPE or choroidal atrophy.

the whole genome data of 800 individuals with no history of IRD did not detect the p.Glu34Lys variant in *IFT43*. In addition, screening the whole exome variant data of 1771 individuals from IRD pedigrees with Pakistani, Indian, Middle Eastern, Japanese and Caucasian ethnicity did not detect any pathogenic variants in *IFT43* segregating with disease. Furthermore, screening the whole genome sequence data of 460 individuals from 120 IRD pedigrees from the above populations also did not identify potential candidate variants in *IFT43*, suggesting the uncommon nature of the involvement of *IFT43* mutations in causing IRD.

Expression profile of *IFT43*

Currently, no evidence has been reported for a role of *IFT43* in the retina. Analysis of *IFT43* expression in the retina was studied by RT-PCR and immunohistochemistry (IHC). qRT-PCR analysis of mouse ocular tissues revealed the expression profile for *IFT43* in a 2-month-old mouse with a high level of expression in the retina and minimal expression in the RPE (Fig. 5B). IHC of IFT43 in mouse and human retinal tissue showed that IFT43 is localized predominantly to the photoreceptor outer segment region (Fig. 6). Significant expression was not observed in other layers of the retina. The expression of IFT43 in the retina supports the involvement of this gene in retinal dystrophy.

Expression and localization of wild type and mutant IFT43 in mammalian cells

mIMCD3 cells were transfected with mammalian constructs containing wt-*IFT43* (Fig. 7A–C) or the Glu34Lys-*IFT43* variant (Fig. 7D–F), both tagged with 6X-His. Cells transfected with wt-*IFT43* showed cilia of normal length and the localization of IFT43 at the distal tip of cilia as reported previously (26). Localization of some intraflagellar transport proteins (IFTs) also varies at different stages of the cell division cycle (27). Cells transfected with Glu34Lys-*IFT43* had cilia that were significantly shorter in length ($P < 0.0001$) (Supplementary Material, Fig. S1). mIMCD3 cells transfected with wild type and mutant *IFT43* constructs were stained with IFT88 and acetylated alpha-tubulin antibodies. Acetylated alpha-tubulin staining revealed normal ciliary structures in cells transfected with the wild type construct, and IFT88 localized to the basal bodies and the distal tip of the cilia as previously reported (Fig. 8A–C) (27). In contrast, acetylated tubulin and IFT88 staining showed shorter to no signal of ciliary structures and colocalization of IFT88 with

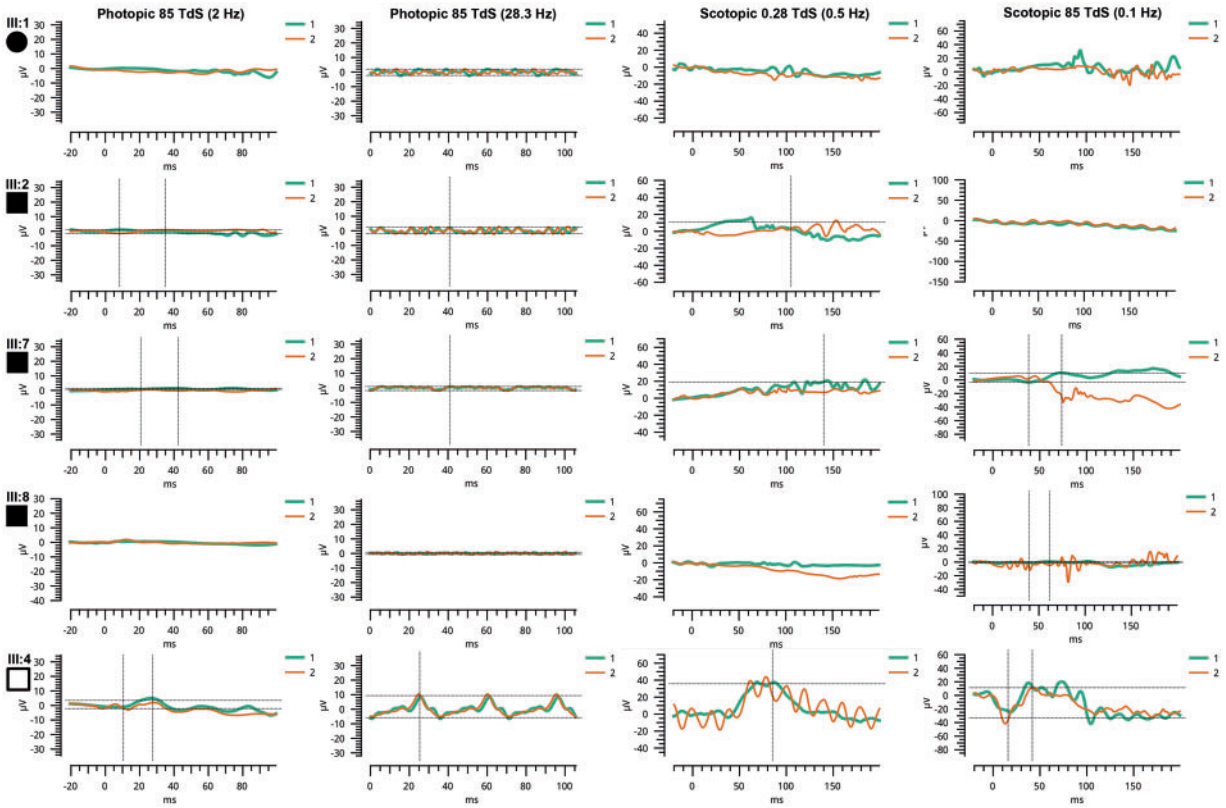

Figure 3. ERG response of members of pedigree PKRD272. Electroretinograms of four affected and one unaffected individuals of pedigree PKRD272 are presented: ERG responses of affected members (III: 1, III: 2, III: 7 and III: 8) were undetectable where as the unaffected individual III: 4 showed normal rod and cone responses.

acetylated tubulin signals in cells transfected with Glu34Lys-*IFT43* (Fig. 8D–F). Similar findings were observed when MDCK cells were transfected with wild-type and mutant *IFT43* constructs (data not shown). Mock-transfected cells did not show immunostaining with 6x-His antibody.

A transfection efficiency of ~70% in cells transfected with both wild type and mutant *IFT43* was observed. Western blot analysis showed the expression of wild type and mutant IFT43 in transiently transfected cells (Supplementary Material, Fig. S2). The presence of an increased amount of protein was observed in the lane loaded with the Glu34Lys-IFT43 compared with the wild type. This finding suggests the possible formation of higher molecular weight aggregates and accumulation of mutant protein in cells expressing mutant IFT43 (28–30). While a detailed analysis is needed to understand the fate and influence of the mutant protein in cells, the findings suggest that the p.Glu34Lys mutation disrupts the intraflagellar transport machinery causing abnormal cilium structure and/or affects ciliogenesis.

Discussion

Homozygosity mapping and whole exome sequencing in a four-generation pedigree PKRD272 identified a novel, potentially pathogenic homozygous change (p.Glu34Lys) in *IFT43* located on chromosome 14. This variant segregated with the early onset retinal degeneration phenotype (Figs 1–3), likely consistent with severe early childhood onset retinal dystrophy (SECORD, ICD-10 H35.5) (31–33) or early onset retinitis pigmentosa (RP) (34). The history of night blindness before age 5 suggests rod cone degeneration, but as adults' full-field ERG responses were not measurable to either scotopic or photopic stimuli and macular atrophy was present. Although the full-field ERGs were not recorded according to International Society for Clinical Electrophysiology of Vision (ISCEV) standards (35), responses were severely reduced to bright and dim stimuli in both dark and light adapted conditions, consistent with the clinical diagnosis of severe early childhood onset retinal dystrophy. The current report adds *IFT43* mutations to the genes that have been associated with early onset RP and macular atrophy, including *NMNAT1*, *AIPL1*, and *LCA5* (36–39).

Previously, a homozygous missense mutation in the *IFT43/C14orf179* was observed in a consanguineous family of Moroccan descent with two siblings diagnosed with Sensenbrenner syndrome (21,40). Remarkably, clinical retinal abnormalities have not been observed in the Moroccan family to date (age 13yrs) (personal communication, Ernie Bongers) (21). Sensenbrenner syndrome is a rare genetically heterogeneous inherited disorder with the involvement of multiple organ systems (19,20). While retinal involvement has not been reported as a common occurrence in Sensenbrenner syndrome, it has been described in a few unrelated families (11,17,18). Although the underlying molecular cause of the disease is unknown in most of these Sensenbrenner patients, Bredrup et al, reported one family with compound heterozygous mutations in *WDR19* encoding *IFT144* (11). One homozygous start loss mutation c.2 T > A (p.Met1Lys) and another homozygous missense c.535 T > C (p.Trp179Arg) mutation in *IFT43* were reported with Short rib polydactyly syndrome in two different families of European descent. The clinical studies on affected cases in these families were performed on fetuses of 18 weeks gestational age and they were reported with

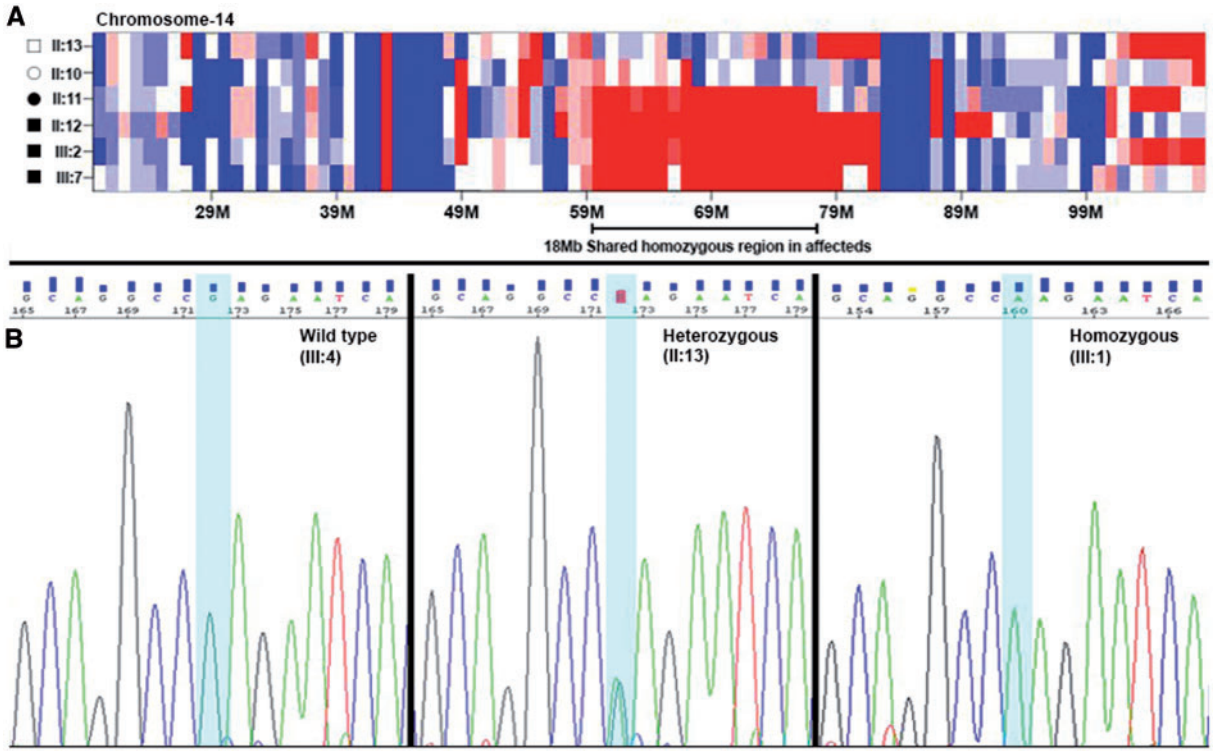

Figure 4. Homozygosity Mapping and Electropherograms of the region containing the c.100 G > A mutation. (**A**) Homozygosity mapping identified one 18 Mb homozygous region on chromosome 14 (chr14: 59000001-77000000), shared by four affected individuals in PKRD272. The alleles of variants in the region depicted in red are homozygous, the region in blue are heterozygous alleles, while the region in white contains homozygous and heterozygous alleles in the same frequency. (**B**) Electropherograms showing the sequence of *IFT43* at the site of c.100 G > A mutation observed in members of PKRD272. The sequence of the region encompassing the *IFT43* c.100 G > A mutation in affected (III: 1), carrier (II: 13) and unaffected (III: 4) individuals from the pedigree PKRD272.

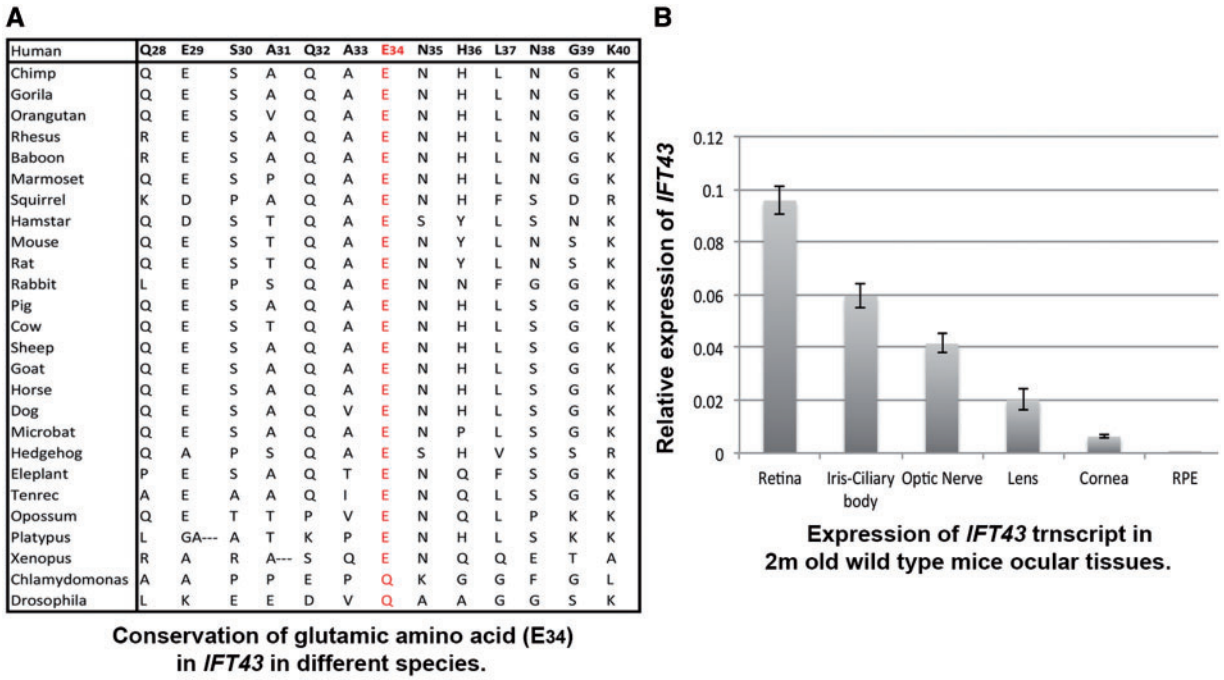

Human	Q28	E29	S30	A31	Q32	A33	E34	N35	H36	L37	N38	G39	K40
Chimp	Q	E	S	A	Q	A	E	N	H	L	N	G	K
Gorila	Q	E	S	A	Q	A	E	N	H	L	N	G	K
Orangutan	Q	E	S	V	Q	A	E	N	H	L	N	G	K
Rhesus	R	E	S	A	Q	A	E	N	H	L	N	G	K
Baboon	R	E	S	A	Q	A	E	N	H	L	N	G	K
Marmoset	Q	E	S	P	Q	A	E	N	H	L	N	G	K
Squirrel	K	D	P	A	Q	A	E	N	H	F	S	D	R
Hamstar	Q	D	S	T	Q	A	E	S	Y	L	S	N	K
Mouse	Q	E	S	T	Q	A	E	N	Y	L	N	S	K
Rat	Q	E	S	T	Q	A	E	N	Y	L	N	S	K
Rabbit	L	E	P	S	Q	A	E	N	N	F	G	G	K
Pig	Q	E	S	A	Q	A	E	N	H	L	S	G	K
Cow	Q	E	S	T	Q	A	E	N	H	L	S	G	K
Sheep	Q	E	S	A	Q	A	E	N	H	L	S	G	K
Goat	Q	E	S	A	Q	A	E	N	H	L	S	G	K
Horse	Q	E	S	A	Q	A	E	N	H	L	S	G	K
Dog	Q	E	S	A	Q	V	E	N	H	L	S	G	K
Microbat	Q	E	S	A	Q	A	E	N	P	L	S	G	K
Hedgehog	Q	A	P	S	Q	A	E	S	H	V	S	S	R
Eleplant	P	E	S	A	Q	T	E	N	Q	F	S	G	K
Tenrec	A	E	A	A	Q	I	E	N	Q	L	S	G	K
Opossum	Q	E	T	T	P	V	E	N	Q	L	P	K	K
Platypus	L	GA---	A	T	K	P	E	N	H	L	S	K	K
Xenopus	R	A	R	A---	S	Q	E	N	Q	Q	E	T	A
Chlamydomonas	A	A	P	P	E	P	Q	K	G	G	F	G	L
Drosophila	L	K	E	E	D	V	Q	A	A	G	G	S	K

Conservation of glutamic amino acid (E34) in *IFT43* in different species.

Figure 5. Conservation of glutamic acid (p.Glu34) and expression profile of *IFT43* in ocular tissues. (**A**) Conserved region surrounding the glutamic acid (p.Glu34) in different species. The glutamic acid residue of p.Glu34Lys is located in a conserved region across different species. (**B**) The *IFT43* transcript showed a high level of expression in retinal tissue as compared with other ocular tissue in 2-month-old mice.

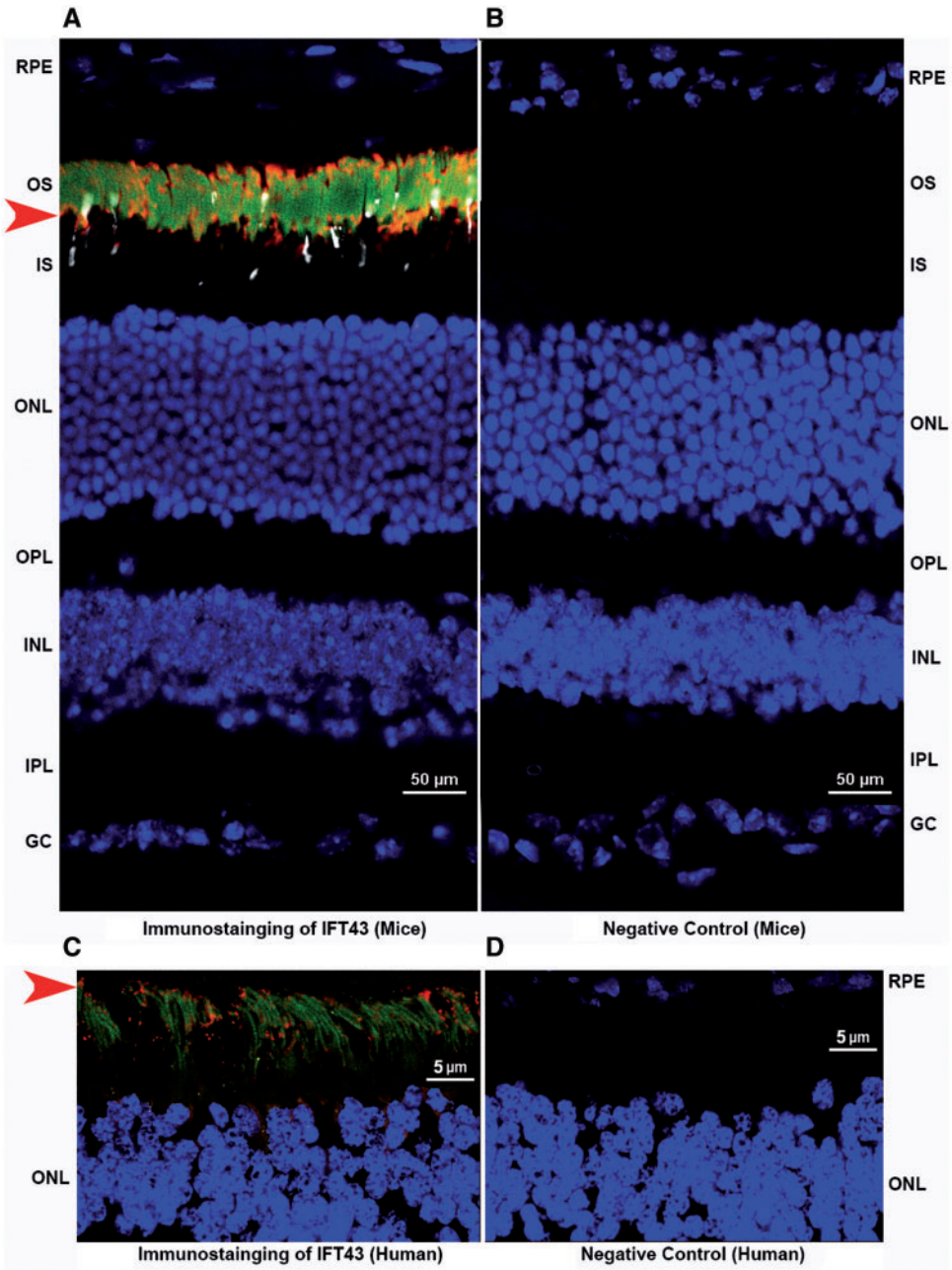

Figure 6. Expression profile of IFT43 in mouse and human retina. Immunostaining of retinal sections of a 6-month-old mouse and a 57-year-old human donor revealed IFT43 localized predominantly to the photoreceptor region of the retina (**A** and **C**). IFT43 was stained and observed in the red channel and indicated by the red arrow. Rhodopsin (green) and S-Opsin (white) are stained with specific antibodies and nuclei are stained with DAPI (blue). Immunostaining of mouse and human retinal sections with secondary antibodies alone did not reveal positive staining (**B** and **D**). RPE, Retinal pigment epithelium; OS, Outer Segments; ONL, Outer Nuclear Layer; OPL, Outer Plexiform Layer; INL, Inner nuclear layer; IPL, Inner Plexiform Layer; GC, Ganglion Cell Layer.

hypertelorism. The influence of *IFT43* mutations on their retina is not known (20). The retinal degeneration phenotype of PKRD272 and the absence of non-ocular abnormalities indicate that the phenotype associated with the *IFT43* p.Glu34Lys mutation is distinctly different from the syndromic phenotypes reported in patients with other *IFT43* gene alterations (21,40). Furthermore, these findings also suggest that individuals with Sensenbrenner syndrome and IFT43 mutations may be at risk for developing blindness although the affected patients in the current study were affected with night vision loss before age 5 and had severe vision loss in adulthood.

The lack of a syndromic phenotype in members of this Pakistani family with the *IFT43* homozygous p.Glu34Lys mutation is intriguing. Similarly, retinal dystrophy has not been reported in patients with Sensenbrenner syndrome due to *IFT43* mutations. Genes associated with cranio ectodermal dysplasia include *IFT43*, *IFT52*, *WDR35/IFT121*, *WDR19/IFT144* and *IFT122* (41–44). All of these are ciliary proteins and members of intraflagellar transport machinery (45). Abnormal retrograde transport of ciliary proteins due to mutations in these genes has been implicated as the underlying cause of the phenotype (41,43,44). *IFT43* is a member of the IFT-A complex that is highly conserved

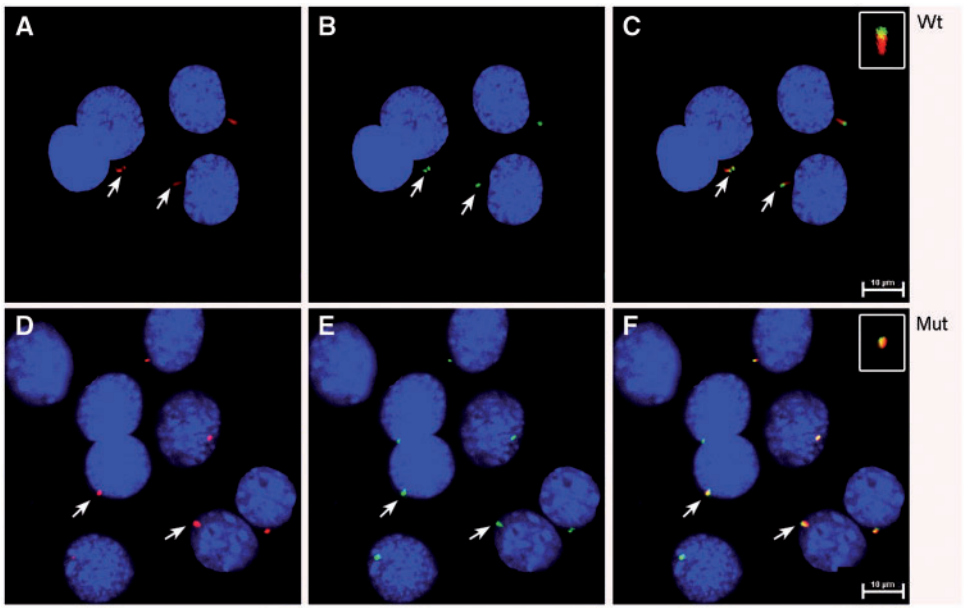

Figure 7. Expression and localization of wt and Glu34Lys-IFT43 in mIMCD3 cells. (**A**) mIMCD3 cells transfected with wt-*IFT43* showed normal appearing cilia when stained with acetylated α-tubulin antibodies (red). (**B**) The wt-IFT43-6X-His fusion protein is localized at the tip of the cilia (green). (**C**) Merged image of A and B. (**D**) Cells transfected with Glu34Lys-*IFT43* showed shortened cilia (red). (**E**) Co-localization of acetylated α-tubulin (red) and mut-IFT43-6X-His (green) in cells transfected with Glu34Lys-*IFT43*. (**F**) Merged image of D and E.

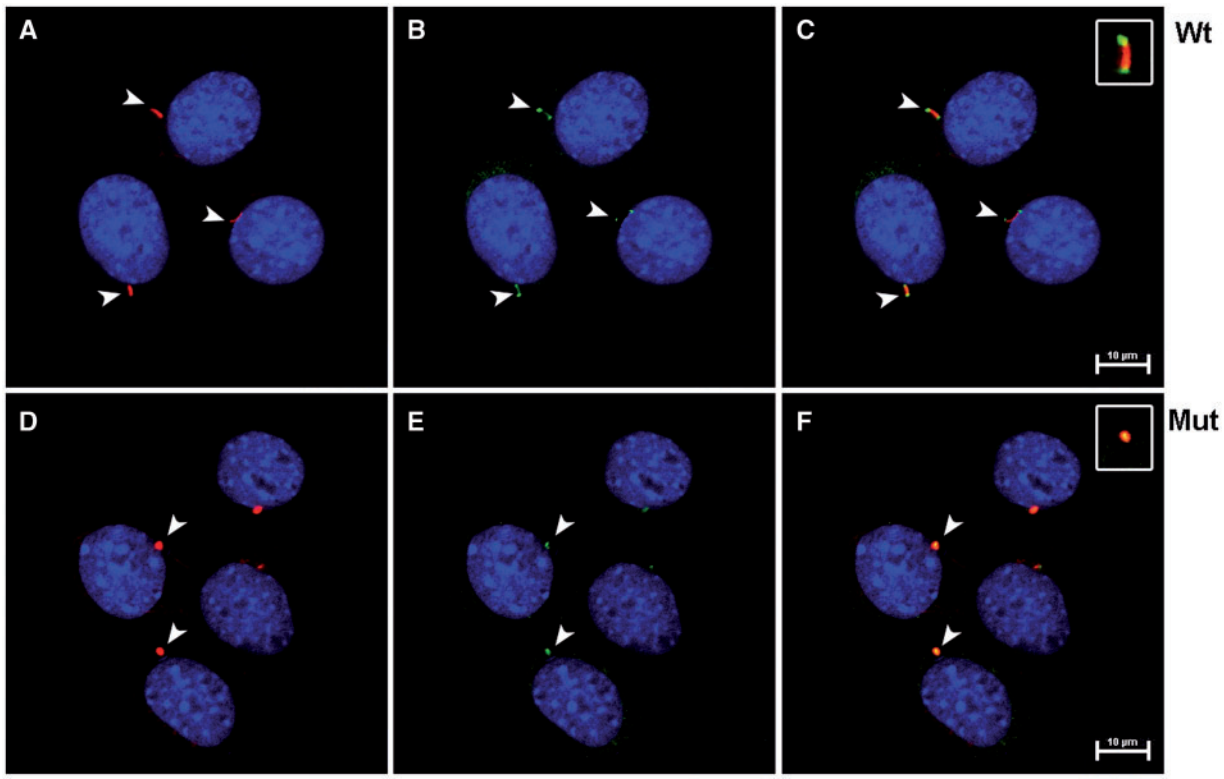

Figure 8. Shortened cilia in mIMCD3 cells transfected with the Glu34Lys-*IFT43*. (**A**) mIMCD3 cells transfected with wt *IFT43* were stained with the ciliary marker protein acetylated α-tubulin (red). (**B**) Intraflagellar transport protein IFT88 (green) is localized to the base and the tip of cilia. (**C**) Merged image of A and B. (**D**) Cells transfected with Glu34Lys-*IFT43* showed shortened cilia (red). (**E**) Co-Staining of acetylated α-tubulin (red) and IFT88 (green) in cells transfected with Glu34Lys-*IFT43* showed shortened cilia. (**F**) Merged image of (D) and (E).

through evolution and interacts closely with *IFT121* (45,46). The specific function of *IFT43* is unknown and no putative structural domains have been identified in this protein, although the proline rich N-terminal half of *IFT43* may play an important role in protein-protein interactions (46). The start codon mutation c.1 A > G; p.Met1Val in the *IFT43* gene found in the Moroccan patients likely results in the utilization of a downstream initiation codon and generation of a mutant protein shorter by 21 amino acids (21). This mutation causes accumulation of *IFT88*, suggesting disruption of retrograde transport of ciliary proteins (21). Similarly, fibroblasts of the patient with a 4.5 Mb heterozygous microdeletion on chromosome 14 showed abnormal transport of ciliary proteins; this suggests that haploinsufficiency of *IFT43* may impact transport of ciliary proteins as well (40). However, the ciliary structures appear to be normal in the fibroblasts of patients with the start codon (c.1 A > G) mutation and the patient with the heterozygous deletion suggesting normal ciliogenesis (21,40). Contrary to these findings, the fibroblasts from SRPS patients with the homozygous p.Trp179Arg mutation showed abnormal ciliogenesis (20). Consistent with these findings, the cells expressing the p.Glu34Lys mutant *IFT43* had significantly shorter ciliary structures indicating abnormal ciliogenesis (Fig. 8 and Supplementary Material, Fig. S1). The missense mutations p.Trp179Arg and p.Glu34Lys mutations may alter the secondary structure of the IFT43 protein leading to abnormal ciliogenesis. Lack of information on the retinal status of the patient with p.Trp179Arg is a limitation, the abnormal ciliogenesis due to the p.Glu34Lys may lead to the retinal degeneration observed in the pedigree PKRK272. Although the mechanism underlying selective retinal degeneration due to the p.Glu34Lys mutation is not known, the absence of pathological changes in non-ocular tissue in affected individuals III: 1, III: 2, III: 7 and III: 8 indicate that photoreceptors may be more sensitive to the p.Glu34Lys mutation than other cells in the body. Photoreceptor cells have a highly evolved ciliary structure that plays a critical role in the development and maintenance of these polarized cells with unique morphology (47–49). The members of IFT machinery participate in ciliogenesis in addition to their role in the bidirectional transport of ciliary proteins in photoreceptors (45,50,51). So far, mutations in four additional members of IFT machinery: *IFT27*, *IFT172*, *IFT140* and *IFT144* have been reported in patients with retinal degenerations (11,52–54). *IFT172* and *IFT140* are involved in causing both syndromic and non-syndromic RD while mutations in *IFT27* and *IFT144* are reported only in syndromic RD. The current understanding of IFT function and the impact of its mutations are not sufficient to explain the variation in syndromic and non-syndromic phenotypes. Similar to *IFT43*, other IRD genes such as *USH2A* and Bardet Biedl syndrome (*BBS*) genes are also implicated in both syndromic and non-syndromic IRD and the mechanism underlying this variation in phenotype is not understood. Future studies of the role of *IFT43* and the impact of its mutations, particularly in photoreceptors cells and animal models, may facilitate a better understanding of the mechanism underlying syndromic and non-syndromic phenotypes associated with mutations in *IFT43* and other IRD genes.

Materials and Methods

Ethics statement

All studies were performed in accordance with the Declaration of Helsinki and the approval of the institutional review boards (IRB) of University of California San Diego, La Jolla, Johns Hopkins University, Baltimore and the National Center of Excellence in Molecular Biology, Lahore, Pakistan. Written informed consent was obtained from all participating subjects. Blood samples were collected from seventeen members of a family (PKRD272) with multiple affected members and multiple consanguineous marriages from Lahore, Pakistan (Fig. 1).

Clinical evaluation

Clinical analysis including electroretinography (ERG), fundus photography, and color vision was performed on four affected members (III: 1, III: 2, III: 7 and III: 8) and two unaffected members of this pedigree (III: 4 and III: 5) (Fig. 1) (55). Patients' ERG responses were measured at 0 dB while the 30 Hz flicker responses were recorded at 0 dB to a background illumination of 17 to 34 cd/m^2 using LKC Technologies, Inc (Gaithersburg, MD).

Genetic analysis

DNA isolation for all available members was performed using Puregene Blood Kit and protocol (Cat No./ID: 158389). Exomes of one affected member (II: 12) were sequenced using Nimblegen V2 kit. Another three affected (II: 11, III: 2 and III: 7) and two unaffected (II: 10 and II: 13) individuals were captured using Nimblegen V3 probe capture kit (Fig. 1). Read mapping and variant calling was performed using BWA and GATK (56). Variants were filtered using exomeSuite as described previously (22). Homozygosity mapping was performed using rare SNPs and INDELs (allele frequency in 1000Genome < 0.001) identified in each 1Mbp window of the genome from four affected and two unaffected individuals (57). Segregation analysis and screening of ethnicity-matched controls were performed by Sanger's dideoxynucleotide sequencing (55).

Expression of *IFT43* transcript

Eyes from 2-month-old wild-type C57BL/6 mice were isolated and dissected to collect different ocular tissues. Isolation of RNA was performed by Qiagen RNeasy® Mini Kit (Cat No./ID: 74104) following standard protocol. Reverse transcription and calculation of *Ift43* expression relative to the housekeeping genes *Gapdh* and *Actb* were performed as described previously (58).

Immunohistochemistry

Cryosections of 6-month-old wild-type C57BL/6 mouse eye and a 57-year-old normal human donor eye were used to perform immunohistochemistry as described previously (59). Rabbit polyclonal anti-IFT43 antibody (1: 100) (Abgent-AP5370c), Anti mouse Rhodopsin (1: 200) (ab3267, Abcam, Cambridge, MA), Anti goat polyclonal OPN1SW (1: 200) (Santa Cruz Biotechnology, Dallas, Texas), AlexaFluor-647-conjugated donkey anti-rabbit secondary antibody (1: 3000) (Invitrogen, Carlsbad, CA, USA), AlexaFluor-488-conjugated donkey anti-mouse secondary antibody (1: 2000) (Invitrogen, Carlsbad, CA, USA) and AlexaFluor-555-conjugated donkey anti-goat secondary antibody (1: 3000) (Invitrogen, Carlsbad, CA, USA) were utilized for staining. Images were captured using Nikon confocal microscope system (A1R+ STORM, Nikon; Melville, NY 11747, USA) and processed using Adobe Photoshop CS6.

Constructs design for mammalian cell transfections

The image clone containing full-length human *IFT43* (hIFT43 ENST00000238628.10) cDNA [Clone MGC: 16028 (IMAGE: 3608220)] in the pOTB7 plasmid was purchased from PlasmID Repository at Harvard Medical School (Boston, MA 02115). The sequence of the clone was verified using 5'- GAGATGGAGGAT TTGCTCGAC -3' forward primer and 5'- CAGGTGTGCCTGGCC TGCC -3' reverse primer. The point mutation (p.Glu34Lys) was introduced by site-directed mutagenesis using primers 5'- GGAGTCAGCGCAGGCC**A**AGAATCACCTCAATGGCAAGAATTCC -3' and 5'- GGAATTCTTGCCATTGAGGTGATTCT**T**GGCCTGCGCT GACTCC -3'. The PCR product was purified using Zymoclean™ Gel DNA Recovery Kit (Zymogen Research, Irvine, CA, USA) and ligated using Gibson cloning (Gibson Assembly Cloning Kit, NEB). Subsequently, the wt-*IFT43* and Glu34Lys-*IFT43* constructs were generated in pDONR™P1-P4 and pDONR™P3-P2 vector using the Multisite Gateway Cloning Kit (Life Technologies, Carlsbad, CA, USA). The wt-*IFT43* and Glu34Lys-*IFT43* constructs were tagged with polyhistidine at the N-terminus.

Subcellular localization and expression

mIMCD3 cells and MDCK cells were transfected with recombinant expression vectors containing wild type or mutant inserts using Neon® Transfection System (Life Technologies, Carlsbad, CA, USA) as described earlier (30). After 24 h of transfection, cells were collected for further analysis. Immunofluorescence analysis of transfected cells was performed as described earlier (30). Anti-6X His tag® antibody - ChIP Grade (ab9108) antibody (1: 200) (Cambridge, MA 02139-1517), rabbit polyclonal anti-IFT88 antibodies (13967-1-AP) (1: 200) (Proteintech Group, Inc, Rosemont, IL 60018, USA), mouse monoclonal acetylated α-tubulin antibody (sc-23950) (1: 200) (Santa Cruz Biotechnologies, Dallas, TX 75220, USA), donkey-anti-mouse Alexa-Fluor-555 (1: 3000) (Invitrogen, Carlsbad, CA, USA) and donkey anti-rabbit secondary antibody Alexa-Fluor-488 (1: 2000) (Invitrogen, Carlsbad, CA, USA) were used for immunostaining. Images were captured using Nikon confocal microscope system (A1R STORM, Melville, NY, USA). The intracellular localization of wt-IFT43 and Glu34Lys-IFT43 proteins were compared relative to the ciliary marker acetylated-α-tubulin. Image J64 software was used for measuring the length of the cilia in at least 50 transfected cells of each type.

Analysis of wild type and mutant IFT43 protein in transfected cells

Expression of wild type and mutant IFT43 in transiently transfected mIMCD3 cells was evaluated by western blot analysis using anti-6X His tag® antibody - ChIP Grade (ab9108) antibody (1: 2000) (Cambridge, MA 02139-1517) and chicken anti-rabbit IgG-HRP (1: 3000) (sc-2963). After stripping, the membrane was reprobed with monoclonal anti-b-Actin, Clone AC-74 primary antibody (1: 2000) (Sigma Aldrich) and bovine anti-mouse IgG-HRP (1: 3000) (sc-2963). The images of the immunoblots were captured using MyECL gel Imager (Thermo Fisher Scientific) and processed using Adobe Photoshop CS6.

Supplementary Material

Supplementary Material is available at *HMG* online.

Acknowledgements

We would like to thank all the individuals for participating in this research study. We are also grateful to Carlo Rivolta, Department of Medical Genetics, University of Lausanne, Lausanne, Switzerland and Fowzan Alkuray, King Faisal Specialist Hospital and Research Center, Riyadh, Saudi Arabia for screening the database of variants observed in their study cohorts for sequence alterations in *IFT43*.

Conflict of Interest statement. None declared.

Funding

The Foundation Fighting Blindness, Research to Prevent Blindness (unrestricted grant to UCSD, UCSF and the Nelson Trust Award for Retinitis Pigmentosa), Bright Focus Foundation, National Eye Institute Grants (NIH-EY21237, P30-EY22589, P30 2P30CA023100).

Web References

1. Ensemble Genome Browser: http://uswest.ensembl.org/index.html
2. RetNet: http://www.sph.uth.tmc.edu/Retnet/
3. Gene Card: http://www.genecards.org
4. UCSC Genome Browser: http://genome.ucsc.edu/cgi-bin/hgGateway
5. UniGene: https://www.ncbi.nlm.nih.gov/unigene

References

1. Heckenlively, J.R. (1988) *Retinitis Pigmentosa*. J.B. Lippincott Company, Philadelphia.
2. Hartong, D.T., Berson, E.L. and Dryja, T.P. (2006) Retinitis pigmentosa. *Lancet*, **368**, 1795–1809.
3. Da Pozzo, P., Cardaioli, E., Malfatti, E., Gallus, G.N., Malandrini, A., Gaudiano, C., Berti, G., Invernizzi, F., Zeviani, M. and Federico, A. (2009) A novel mutation in the mitochondrial tRNA(Pro) gene associated with late-onset ataxia, retinitis pigmentosa, deafness, leukoencephalopathy and complex I deficiency. *Eur. J. Hum. Genet.*, **17**, 1092–1096.
4. Fahim, A.T., Daiger, S.P. and Weleber, R.G. (1993) Pagon, R.A., Adam, M.P., Ardinger, H.H., Wallace, S.E., Amemiya, A., Bean, L.J.H., Bird, T.D., Fong, C.T., Mefford, H.C., Smith, R.J.H. and Stephens, K. (eds.), *Nonsyndromic Retinitis Pigmentosa Overview*. GeneReviews(R), University of Washington, Seattle (WA), PMID: 20301590, in press.
5. Avila-Fernandez, A., Cantalapiedra, D., Aller, E., Vallespin, E., Aguirre-Lamban, J., Blanco-Kelly, F., Corton, M., Riveiro-Alvarez, R., Allikmets, R., Trujillo-Tiebas, M.J. *et al.* (2010) Mutation analysis of 272 Spanish families affected by autosomal recessive retinitis pigmentosa using a genotyping microarray. *Mol. Vis.*, **16**, 2550–2558.
6. Farber, D.B., Heckenlively, J.R., Sparkes, R.S. and Bateman, J.B. (1991) Molecular genetics of retinitis pigmentosa. *West. J. Med.*, **155**, 388–399.
7. Espinos, C., Perez-Garrigues, H., Beneyto, M., Vilela, C., Rodrigo, O. and Najera, C. (1999) [Syndromic hereditary deafness. Usher's syndrome. Oto-neurologic and genetic factors]. *An. Otorrinolaringol. Ibero. Am.*, **26**, 83–95.
8. Blaydon, D.C., Mueller, R.F., Hutchin, T.P., Leroy, B.P., Bhattacharya, S.S., Bird, A.C., Malcolm, S. and Bitner-Glindzicz, M. (2003) The contribution of USH1C mutations to

syndromic and non-syndromic deafness in the UK. *Clin. Genet.*, **63**, 303–307.
9. Li, J.B., Gerdes, J.M., Haycraft, C.J., Fan, Y., Teslovich, T.M., May-Simera, H., Li, H., Blacque, O.E., Li, L., Leitch, C.C. *et al.* (2004) Comparative genomics identifies a flagellar and basal body proteome that includes the BBS5 human disease gene. *Cell*, **117**, 541–552.
10. Young, T.L., Penney, L., Woods, M.O., Parfrey, P.S., Green, J.S., Hefferton, D. and Davidson, W.S. (1999) A fifth locus for Bardet-Biedl syndrome maps to chromosome 2q31. *Am. J. Hum. Genet.*, **64**, 900–904.
11. Bredrup, C., Saunier, S., Oud, M.M., Fiskerstrand, T., Hoischen, A., Brackman, D., Leh, S.M., Midtbo, M., Filhol, E., Bole-Feysot, C. *et al.* (2011) Ciliopathies with skeletal anomalies and renal insufficiency due to mutations in the IFT-A gene WDR19. *Am. J. Hum. Genet.*, **89**, 634–643.
12. Chaki, M., Airik, R., Ghosh, A.K., Giles, R.H., Chen, R., Slaats, G.G., Wang, H., Hurd, T.W., Zhou, W., Cluckey, A. *et al.* (2012) Exome capture reveals ZNF423 and CEP164 mutations, linking renal ciliopathies to DNA damage response signaling. *Cell*, **150**, 533–548.
13. Adams, N.A., Awadein, A. and Toma, H.S. (2007) The retinal ciliopathies. *Ophthalmic Genet.*, **28**, 113–125.
14. Delous, M., Baala, L., Salomon, R., Laclef, C., Vierkotten, J., Tory, K., Golzio, C., Lacoste, T., Besse, L., Ozilou, C. *et al.* (2007) The ciliary gene RPGRIP1L is mutated in cerebello-oculo-renal syndrome (Joubert syndrome type B) and Meckel syndrome. *Nat. Genet.*, **39**, 875–881.
15. Badano, J.L., Ansley, S.J., Leitch, C.C., Lewis, R.A., Lupski, J.R. and Katsanis, N. (2003) Identification of a novel Bardet-Biedl syndrome protein, BBS7, that shares structural features with BBS1 and BBS2. *Am. J. Hum. Genet.*, **72**, 650–658.
16. Badano, J.L., Kim, J.C., Hoskins, B.E., Lewis, R.A., Ansley, S.J., Cutler, D.J., Castellan, C., Beales, P.L., Leroux, M.R. and Katsanis, N. (2003) Heterozygous mutations in BBS1, BBS2 and BBS6 have a potential epistatic effect on Bardet-Biedl patients with two mutations at a second BBS locus. *Hum. Mol. Genet.*, **12**, 1651–1659.
17. Eke, T., Woodruff, G. and Young, I.D. (1996) A new oculorenal syndrome: retinal dystrophy and tubulointerstitial nephropathy in cranioectodermal dysplasia. *Br. J. Ophthalmol.*, **80**, 490–491.
18. Savill, G.A., Young, I.D., Cunningham, R.J., Ansell, I.D. and Evans, J.H. (1997) Chronic tubulo-interstitial nephropathy in children with cranioectodermal dysplasia. *Pediatr. Nephrol.*, **11**, 215–217.
19. Young, I.D. (1989) Cranioectodermal dysplasia (Sensenbrenner's syndrome). *J. Med. Genet.*, **26**, 393–396.
20. Duran, I., Taylor, S.P., Zhang, W., Martin, J., Qureshi, F., Jacques, S.M., Wallerstein, R., Lachman, R.S., Nickerson, D.A., Bamshad, M. *et al.* (2017) Mutations in IFT-A satellite core component genes IFT43 and IFT121 produce short rib polydactyly syndrome with distinctive campomelia. *Cilia*, **6**, 7.
21. Arts, H.H., Bongers, E.M., Mans, D.A., van Beersum, S.E., Oud, M.M., Bolat, E., Spruijt, L., Cornelissen, E.A., Schuurs-Hoeijmakers, J.H., de Leeuw, N. *et al.* (2011) C14ORF179 encoding IFT43 is mutated in Sensenbrenner syndrome. *J. Med. Genet.*, **48**, 390–395.
22. Maranhao, B., Biswas, P., Duncan, J.L., Branham, K.E., Silva, G.A., Naeem, M.A., Khan, S.N., Riazuddin, S., Hejtmancik, J.F., Heckenlively, J.R. *et al.* (2014) exomeSuite: Whole exome sequence variant filtering tool for rapid identification of putative disease causing SNVs/indels. *Genomics*, **103**, 169–176.
23. Lek, M., Karczewski, K.J., Minikel, E.V., Samocha, K.E., Banks, E., Fennell, T., O'Donnell-Luria, A.H., Ware, J.S., Hill, A.J., Cummings, B.B. *et al.* (2016) Analysis of protein-coding genetic variation in 60, 706 humans. *Nature*, **536**, 285–291.
24. Adzhubei, I., Jordan, D.M. and Sunyaev, S.R. (2013) Predicting functional effect of human missense mutations using PolyPhen-2. *Curr Protoc Hum Genet.*, **Chapter 7**, Unit7, 20.
25. Ng, P.C. and Henikoff, S. (2003) SIFT: Predicting amino acid changes that affect protein function. *Nucleic Acids Res.*, **31**, 3812–3814.
26. Broekhuis, J.R., Verhey, K.J., Jansen, G. and Stieger, K. (2014) Regulation of cilium length and intraflagellar transport by the RCK-kinases ICK and MOK in renal epithelial cells. *PloS One*, **9**, e108470.
27. Robert, A., Margall-Ducos, G., Guidotti, J.E., Bregerie, O., Celati, C., Brechot, C. and Desdouets, C. (2007) The intraflagellar transport component IFT88/polaris is a centrosomal protein regulating G1-S transition in non-ciliated cells. *J. Cell Sci.*, **120**, 628–637.
28. Johnston, J.A., Ward, C.L. and Kopito, R.R. (1998) Aggresomes: a cellular response to misfolded proteins. *J. Cell Biol.*, **143**, 1883–1898.
29. Markossian, K.A. and Kurganov, B.I. (2004) Protein folding, misfolding, and aggregation. Formation of inclusion bodies and aggresomes. *Biochemistry (Mosc)*, **69**, 971–984.
30. Vasireddy, V., Vijayasarathy, C., Huang, J., Wang, X.F., Jablonski, M.M., Petty, H.R., Sieving, P.A. and Ayyagari, R. (2005) Stargardt-like macular dystrophy protein ELOVL4 exerts a dominant negative effect by recruiting wild-type protein into aggresomes. *Mol. Vis.*, **11**, 665–676.
31. Weleber, R.G., Michaelides, M., Trzupek, K.M., Stover, N.B. and Stone, E.M. (2011) The phenotype of Severe Early Childhood Onset Retinal Dystrophy (SECORD) from mutation of RPE65 and differentiation from Leber congenital amaurosis. *Invest. Ophthalmol. Vis. Sci.*, **52**, 292–302.
32. Mackay, D.S., Ocaka, L.A., Borman, A.D., Sergouniotis, P.I., Henderson, R.H., Moradi, P., Robson, A.G., Thompson, D.A., Webster, A.R. and Moore, A.T. (2011) Screening of SPATA7 in patients with Leber congenital amaurosis and severe childhood-onset retinal dystrophy reveals disease-causing mutations. *Invest. Ophthalmol. Vis. Sci.*, **52**, 3032–3038.
33. Lewis, C.A., Batlle, I.R., Batlle, K.G., Banerjee, P., Cideciyan, A.V., Huang, J., Aleman, T.S., Huang, Y., Ott, J. and Gilliam, T.C. (1999) Tubby-like protein 1 homozygous splice-site mutation causes early-onset severe retinal degeneration. *Invest. Ophthalmol. Vis. Sci.*, **40**, 2106–2114.
34. Foxman, S.G., Heckenlively, J.R., Bateman, J.B. and Wirtschafter, J.D. (1985) Classification of congenital and early onset retinitis pigmentosa. *Arch. Ophthalmol.*, **103**, 1502–1506.
35. McCulloch, D.L., Marmor, M.F., Brigell, M.G., Hamilton, R., Holder, G.E., Tzekov, R. and Bach, M. (2015) ISCEV Standard for full-field clinical electroretinography (2015 update). *Doc. Ophthalmol.*, **130**, 1–12.
36. Falk, M.J., Zhang, Q., Nakamaru-Ogiso, E., Kannabiran, C., Fonseca-Kelly, Z., Chakarova, C., Audo, I., Mackay, D.S., Zeitz, C., Borman, A.D. *et al.* (2012) NMNAT1 mutations cause Leber congenital amaurosis. *Nat. Genet.*, **44**, 1040–1045.
37. Perrault, I., Hanein, S., Zanlonghi, X., Serre, V., Nicouleau, M., Defoort-Delhemmes, S., Delphin, N., Fares-Taie, L., Gerber, S., Xerri, O. *et al.* (2012) Mutations in NMNAT1 cause Leber

congenital amaurosis with early-onset severe macular and optic atrophy. *Nat. Genet.*, **44**, 975–977.
38. Dharmaraj, S., Leroy, B.P., Sohocki, M.M., Koenekoop, R.K., Perrault, I., Anwar, K., Khaliq, S., Devi, R.S., Birch, D.G., De Pool, E. *et al.* (2004) The phenotype of Leber congenital amaurosis in patients with AIPL1 mutations. *Arch. Ophthalmol.*, **122**, 1029–1037.
39. Mohamed, M.D., Topping, N.C., Jafri, H., Raashed, Y., McKibbin, M.A. and Inglehearn, C.F. (2003) Progression of phenotype in Leber's congenital amaurosis with a mutation at the LCA5 locus. *Br. J. Ophthalmol.*, **87**, 473–475.
40. Stokman, M.F., Oud, M.M., van Binsbergen, E., Slaats, G.G., Nicolaou, N., Renkema, K.Y., Nijman, I.J., Roepman, R., Giles, R.H., Arts, H.H. *et al.* (2016) De novo 14q24.2q24.3 microdeletion including IFT43 is associated with intellectual disability, skeletal anomalies, cardiac anomalies, and myopia. *Am. J. Med. Genet. A*, **170**, 1566–1569.
41. Fu, W., Wang, L., Kim, S., Li, J. and Dynlacht, B.D. (2016) Role for the IFT-A complex in selective transport to the primary cilium. *Cell Reports*, **17**, 1505–1517.
42. Girisha, K.M., Shukla, A., Trujillano, D., Bhavani, G.S., Hebbar, M., Kadavigere, R. and Rolfs, A. (2016) A homozygous nonsense variant in IFT52 is associated with a human skeletal ciliopathy. *Clin. Genet.*, **90**, 536–539.
43. Liem, K.F., Jr., Ashe, A., He, M., Satir, P., Moran, J., Beier, D., Wicking, C. and Anderson, K.V. (2012) The IFT-A complex regulates Shh signaling through cilia structure and membrane protein trafficking. *J. Cell Biol.*, **197**, 789–800.
44. Alazami, A.M., Seidahmed, M.Z., Alzahrani, F., Mohammed, A.O. and Alkuraya, F.S. (2014) Novel IFT122 mutation associated with impaired ciliogenesis and cranioectodermal dysplasia. *Mol. Genet. Genomic Med.*, **2**, 103–106.
45. Sedmak, T. and Wolfrum, U. (2010) Intraflagellar transport molecules in ciliary and nonciliary cells of the retina. *J. Cell Biol.*, **189**, 171–186.
46. Behal, R.H., Miller, M.S., Qin, H., Lucker, B.F., Jones, A. and Cole, D.G. (2012) Subunit interactions and organization of the *Chlamydomonas reinhardtii* intraflagellar transport complex A proteins. *J. Biol. Chem.*, **287**, 11689–11703.
47. Roepman, R. and Wolfrum, U. (2007) Protein networks and complexes in photoreceptor cilia. *Subcell. Biochem.*, **43**, 209–235.
48. Bhowmick, R., Li, M., Sun, J., Baker, S.A., Insinna, C. and Besharse, J.C. (2009) Photoreceptor IFT complexes containing chaperones, guanylyl cyclase 1 and rhodopsin. *Traffic*, **10**, 648–663.
49. Horst, C.J., Johnson, L.V. and Besharse, J.C. (1990) Transmembrane assemblage of the photoreceptor connecting cilium and motile cilium transition zone contain a common immunologic epitope. *Cell Motil. Cytoskeleton*, **17**, 329–344.
50. Wang, J. and Deretic, D. (2014) Molecular complexes that direct rhodopsin transport to primary cilia. *Prog. Retin. Eye Res.*, **38**, 1–19.
51. Zhu, B., Zhu, X., Wang, L., Liang, Y., Feng, Q. and Pan, J. (2017) Functional exploration of the IFT-A complex in intraflagellar transport and ciliogenesis. *PLoS Genet.*, **13**, e1006627.
52. Bujakowska, K.M., Zhang, Q., Siemiatkowska, A.M., Liu, Q., Place, E., Falk, M.J., Consugar, M., Lancelot, M.E., Antonio, A., Lonjou, C. *et al.* (2015) Mutations in IFT172 cause isolated retinal degeneration and Bardet-Biedl syndrome. *Hum. Mol. Genet.*, **24**, 230–242.
53. Aldahmesh, M.A., Li, Y., Alhashem, A., Anazi, S., Alkuraya, H., Hashem, M., Awaji, A.A., Sogaty, S., Alkharashi, A., Alzahrani, S. *et al.* (2014) IFT27, encoding a small GTPase component of IFT particles, is mutated in a consanguineous family with Bardet-Biedl syndrome. *Hum. Mol. Genet.*, **23**, 3307–3315.
54. Perrault, I., Saunier, S., Hanein, S., Filhol, E., Bizet, A., Collins, F., Salih, M., Silva, E., Baudouin, V., Oud, M. *et al.* (2012) Mainzer-Saldino syndrome is a ciliopathy caused by IFT140 mutations. *Am. J. Hum. Genet.*, **1**, O28. 864870.
55. Duncan, J.L., Biswas, P., Kozak, I., Navani, M., Syed, R., Soudry, S., Menghini, M., Caruso, R.C., Jeffrey, B.G., Heckenlively, J.R. *et al.* (2014) Ocular phenotype of a family with FAM161A-associated retinal degeneration. *Ophthalmic Genet.*, **37**, 44–52, 1–9.
56. Duncan, J.L., Roorda, A., Navani, M., Vishweswaraiah, S., Syed, R., Soudry, S., Ratnam, K., Gudiseva, H.V., Lee, P., Gaasterland, T. *et al.* (2012) Identification of a novel mutation in the CDHR1 gene in a family with recessive retinal degeneration. *Arch. Ophthalmol.*, **130**, 1301–1308.
57. McKenna, A., Hanna, M., Banks, E., Sivachenko, A., Cibulskis, K., Kernytsky, A., Garimella, K., Altshuler, D., Gabriel, S., Daly, M. *et al.* (2010) The Genome Analysis Toolkit: a MapReduce framework for analyzing next-generation DNA sequencing data. *Genome. Res.*, **20**, 1297–1303.
58. Mandal, M.N., Vasireddy, V., Jablonski, M.M., Wang, X., Heckenlively, J.R., Hughes, B.A., Reddy, G.B. and Ayyagari, R. (2006) Spatial and temporal expression of MFRP and its interaction with CTRP5. *Invest. Ophthalmol. Vis. Sci.*, **47**, 5514–5521.
59. Chavali, V.R., Khan, N.W., Cukras, C.A., Bartsch, D.U., Jablonski, M.M. and Ayyagari, R. (2011) A CTRP5 gene S163R mutation knock-in mouse model for late-onset retinal degeneration. *Hum. Mol. Genet.*, **20**, 2000–2014.